

Fully Inkjet Printed 60GHz Backscatter 5G RFID Modules for Sensing and Localization in Internet of Things (IoT) and Digital Twins Applications

Ajibayo Adeyeye, Charles Lynch, Xuanke He, Sanghoon Lee, John D. Cressler, Manos M. Tentzeris

Department of Electrical and Computer Engineering

Georgia Institute of Technology

Atlanta, Georgia

aaadeyeye3@gatech.edu, clynch42@gatech.edu, xhe53@gatech.edu, sle837@gatech.edu, cressler@ece.gatech.edu, etentze@ece.gatech.edu

Abstract—The exponentially increasing demand for low-cost and high performance wireless devices and modules as a part of the proliferation of the Internet of Things (IoT) and digital twins has made investigation into efficient means of manufacturing and integration of these devices necessary. In this effort, the authors report a simple low cost RFID module operating in the 60GHz Industrial, Scientific and Medical (ISM) band equipped with an ultra sensitive flex sensor. The reported system is capable of detecting continuous flexing of the sensor while simultaneously able to report it's range to within 5 mm of error. In addition to the device presented, this work outlines a simple low cost additive manufacturing procedure that enables integration of the sensor with a communicating node in a single process.

Index Terms—additive manufacturing, inkjet printing, Radar, RFID

I. INTRODUCTION

Over the last decade, there has been a dramatically increased interest in the use of Radio Frequency Identification (RFID) technologies for use in wireless sensing and positioning schemes as part of the burgeoning Internet of Things revolution. This is largely due to it's high energy efficiency which stems from the fact that in the backscatter topology the devices do not generate their own RF signal. Instead, they are activated using only the RF signal generated by illumination from a reader device. In modulated backscatter systems, the tag is interrogated with a continuous wave and it reflects the interrogating wave back to the reader with a dynamic reflection coefficient that is a function of the load presented to the tag antenna at a given time. For use in positioning, the semi-passive backscatter system has been reported for use with Frequency Modulated Continuous Wave (FMCW) radar which enables localization with high fidelity due to increased signal to noise ratio compared to passive targets more commonly localized [1]–[3].

Despite the obvious advantages of this system, there have been numerous roadblocks in realizing the full potential of wide scale deployment and reliable connectivity between devices. Mainly, there are already a large number of existing devices operating in the Ultra High Frequency range (300MHz – 3GHz) and these frequency bands also suffer from limited

available bandwidth as well as radiated power limitations. With the requirements for very large number of devices, current methods of production become untenable as the number of required wireless modules, IoT and digital twins increases exponentially.

Additive manufacturing (AM) presents an attractive, cost saving and more sustainable solution in the long term. Additionally, the rapidly re-configurable nature of AM enables the design and implementation of diverse on-demand application-specific sensor modules with reduced retooling and assembly overhead compared to traditional lithographic techniques. This creates a unique opportunity to combine the advantages of AM techniques with the development of fully additively manufactured wireless modules operating in the millimeter wave frequency regime. AM Techniques such as inkjet and 3D printing have been demonstrated to provide comparable performance to conventional lithography techniques in the fabrication of wireless modules up to the W-band in a variety of key wireless technology enabling applications [4]–[9].

In this effort, a fully inkjet-printed backscatter RFID module operating at 60GHz is proposed. The module consists of an RF front end and associated baseband circuitry. The RF front end includes an inkjet printed 5 element linear patch antenna array, a diode for load modulation to enable backscatter communication as well as printed RF-DC isolation stubs. The baseband circuit is comprised of an oscillator to control the load modulation, a voltage regulator, and an energy source. Inkjet printing technology enables the direct integration of the entire RF front end of the wireless module. An additional advantage of this architecture is the ease with which a variety of on-demand printed wireless can be easily integrated. In this effort, a printed resistance based strain/flex sensor is integrated with the aforementioned backscatter RFID module with it's response encoded in the modulation frequency of the RFID module using a voltage controlled oscillator.

The shift up to the 60GHz band necessitates the use of a reader system operating in this band. Previously, the integration of a large number low cost wireless modules in the millimeter wave regime would be unfeasible due to increased

cost of components and subsequent deployment. However, with the development of single chip low-cost radar modules in these bands there is increased opportunity for integration and wide-scale deployment of these sensing devices. An FMCW enabled radar module is chosen as the means of interrogation due to its low cost and high performance when used in conjunction with modulated backscatter [3].

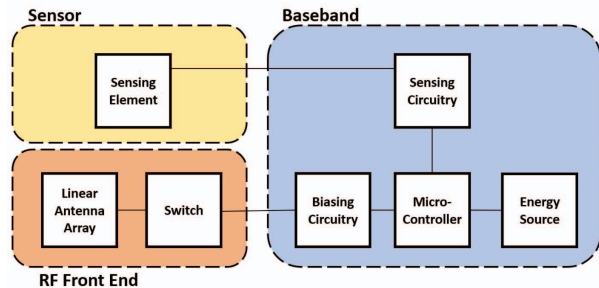


Fig. 1: System level block diagram

II. SYSTEM ARCHITECTURE

The proposed system is comprised of the mmID sensing node and an FMCW radar module. The mmID node consists of three main components namely the RF front end, the sensing element, and the micro-controller unit to extract sensor information and map this waveform to an oscillating frequency to be read wirelessly with the radar module. The reader utilized is the IWR6843AOPEVM radar module from Texas Instruments. This radar module operates from 60 GHz to 64 GHz and contains three transmit and four receive antenna channels. This form-factor Antenna-on-Package module can be viewed in Figure 2.

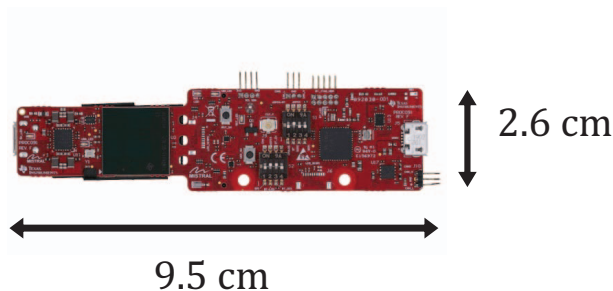


Fig. 2: 60 GHz Radar module used for interrogation

Due to the layout of the antennas and utilizing single elements for transmission and receive, the module exhibits a $\pm 120^\circ$ field-of-view centered at boresight, with each element having 6 dBi of gain. Additionally, with a rated maximum transmitted power of 12 dBm, this module is a cost-effective cheap solution to mm-Wave sensing applications.

A. RF Front-End

In general, the RF front end of a backscattering node consists of an antenna and a load that can be controlled to

present different load states to the terminals of the antenna such that the incident electromagnetic wave can be reflected with a varying reflection coefficient. In this case, the antenna component selected was a 5x1 series-fed patch antenna array. At the input of the array there was a quarter-wave transformer included to match the input impedance of the array to a $50\ \Omega$ transmission line. A measurement of the return loss can be viewed in Figure 4a.

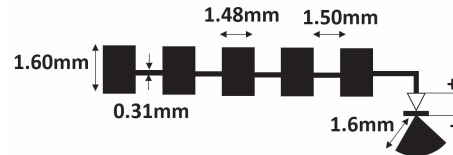


Fig. 3: Schematic of Designed RF Front End.

It can be seen from the measured return loss that the array displays good matching across the entire operational bandwidth of the FMCW radar module. The performance of the radiating element in a backscatter link is pertinent to having an acceptable link budget as the gain of the antenna is integrated both in reception of the interrogating signal and in its reflection back to the reader. However, in the same vein the mismatch losses in the antenna are also integrated both in the forward and return links. Thus, a well matched and high gain antenna was critical for this application.

The switching element utilized for this design was a low-cost MADS-001317-1500 schottky diode from MACOM. The load was designed to operate in binary phase shift keying (BPSK) so that in the zero bias state the reflection coefficient has a phase of 0° and when biased a phase of 180° which essentially appears to be an open and short circuit, respectively. The short circuit was realized using a quarter wavelength long radial stub. The measured phase difference between the zero-bias and 0.9 V state can be viewed in Figure 4b.

The measured phase difference between the two states of the diode show that the device exhibits more than 100° of difference in phase between the two load states across the majority of the required bandwidth.

B. Sensing Element

The sensing element employed in this work was an inkjet printed strain sensor. The sensor was made up of a set of meandered conductive traces which exhibit a linear change in resistance when deformed. This resistive strain sensor has a total layout of 90 by 45 cm and a section can be viewed with its dimensions in Figure 5.

The change in resistance exhibited was minute and thus the sensor was put in a Wheatstone bridge configuration so that the small changes in resistance due to deformation of the sensor could be detected accurately and linearly mapped.

C. Baseband Circuitry

The baseband/DC elements of the proposed module was comprised of four main components namely the micro-

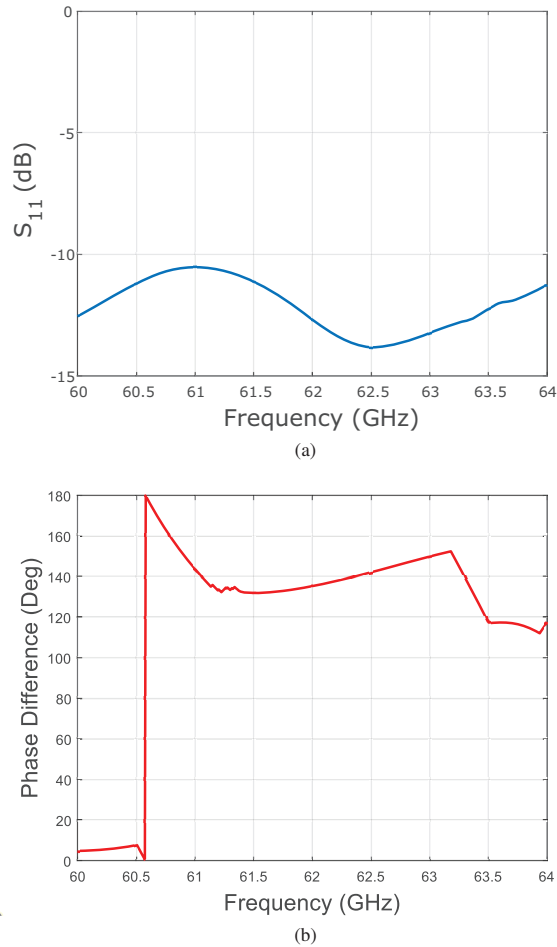


Fig. 4: Reflection amplifier characterization: (a) Return loss of the 5x1 series-fed antenna array.; (b) Phase difference between 0 V and 0.9 V biasing states of low-cost schottky diode.

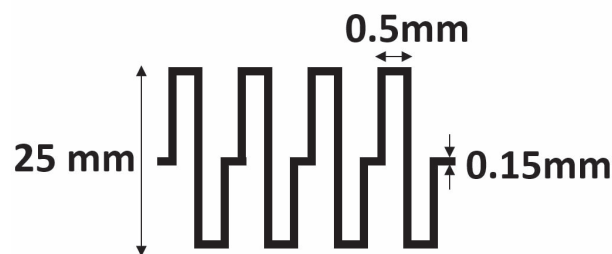


Fig. 5: Section of fabricated sensor

controller, the sensing circuitry, the diode biasing circuitry and an energy source. For the proof of concept work presented here, a power supply was used however for smaller implementations, super-capacitors in conjunction with energy harvesting

circuitry could feasibly be used for low power operation of the system.

The biasing circuit was made up of the LTC6907 micropower resistor set oscillator which was configured to accept a voltage in the range 0 V to 0.675 V and returns a frequency between 400 kHz - 4 MHz. A bias voltage of 0.9 V was chosen for the diode so it was necessary to include a voltage divider to properly scale the 3.3 V oscillator output. The sensing circuit included the Wheatstone bridge connected to the resistive sensing element as well as the micropower INA126 instrumentation amplifier which was used to amplify the minuscule voltage change induced by the change in resistance of the sensing element when deformed.

The micro-controller used was the ATSAM21G18 which tied the system together. It was responsible for reading the amplified input voltage from the sensing circuit and using a linear scale to generate a corresponding output voltage used to drive the biasing circuit and generate the modulating signal. The output voltage generated is set to be between 0 V to 0.129 V so that the voltage controlled oscillator generates a frequency between 3.56 MHz to 3.9 MHz in a linear scale based on the read input voltage. A schematic of the full baseband circuit is shown in Figure 6. The resultant bias voltage V_{bias} is fed to the diode on the RF front end and resistors $R3$ and $R4$ are chosen such that V_{bias} oscillates between 0 V to 0.9 V.

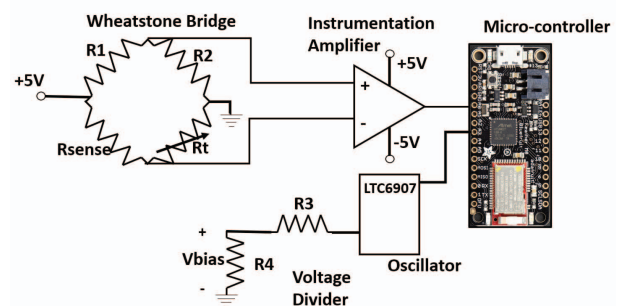


Fig. 6: Baseband circuit schematic

III. DEVICE FABRICATION

The fabrication of the proposed wireless sensing module is achieved in a few steps primarily utilizing inkjet printing technology. The substrate chosen for the proposed device was Kapton HN which was $127\mu\text{m}$ thick and featured a permittivity, $\epsilon_r = 3.5$ and loss tangent, $\tan\delta = 0.0026$. Prior to commencement of the inkjet printing process however, the surface of the Kapton film required treatment to increase its surface roughness and allow the printed silver nanoparticles to adhere better to its surface. This is done by submerging the substrate in a 1 molar Potassium Hydroxide bath for a period of one hour [10]. After this surface treatment, the substrate was then thoroughly rinsed with water, dried, and $35\mu\text{m}$ thick copper tape was adhered to the bottom of the substrate to act as

the ground layer for the RF front end. Next, the pattern files for the RF front end and sensor are loaded onto a Dimatix DMP-2831 inkjet printer. The silver nanoparticle (SNP) based ink used was the EMD5730 from Sun Chemical. Two layers of SNP were printed for the sensor to ensure connectivity and a high enough resistance while 3 layers of SNP were printed for the RF front end. The SNP ink printed was dried between layers to prevent ink spreading to preserve the loaded pattern.

After printing, the diode switching element is placed on the printed pads with a small amount of conductive paste to aid adhesion and then the sample is sintered in an oven at 150 °C for one hour. The final fabricated device is shown in Figure 8.

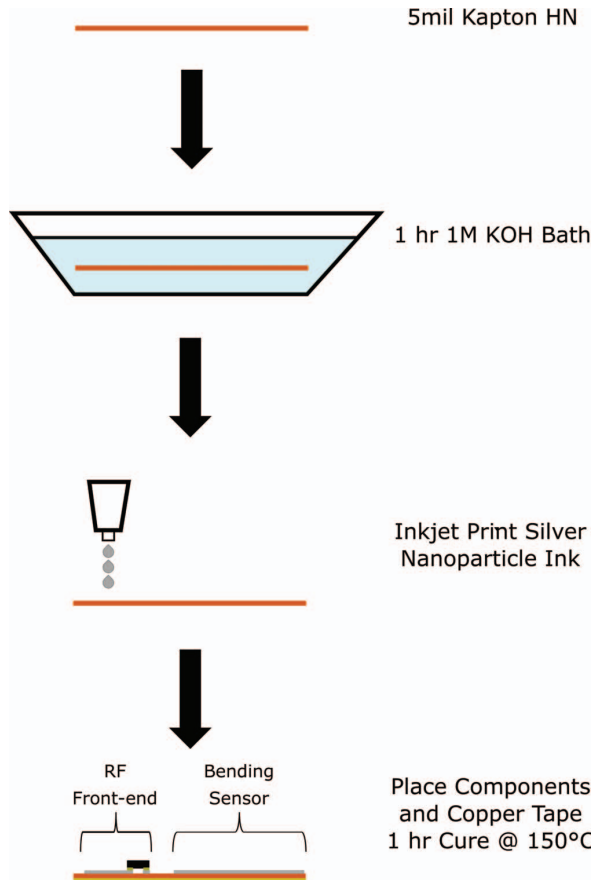


Fig. 7: Fabrication flow of Inkjet Printed 60 GHz mmID tag.

IV. SIMULTANEOUS RANGE AND FLEX SENSING

To benchmark the proposed system’s ability to precisely range and observe local flexing of the digital twin sensor, two categories of measurements were conducted. First, the fabricated sensor was placed at a constant range of 15 cm away from the reader and adhered to three separate cylinders of different radius to enable different levels of flexing. After characterizing the flex sensor response at a constant range from

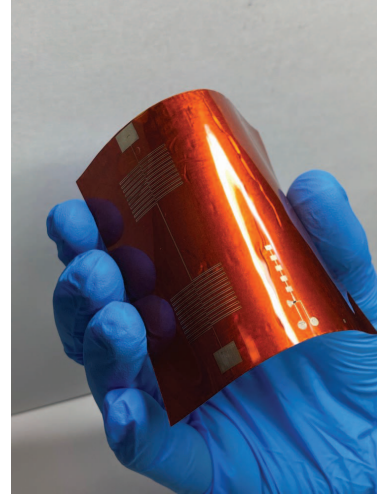


Fig. 8: Fabricated device

TABLE I: Chirp parameters used to acquire the reported measurements.

Parameter	Value
Bandwidth	3.80 GHz
Slope	24.985 MHz/ μ s
Sampling Rate	10 MHz
Chirps per Frame	128
Chirp Periodicity	160 μ s

the reader, the flex sensor was placed on the largest radius cylinder and placed at ranges from 15 cm to 60 cm in steps of 15 cm. The experimental setup of the subsequent measurements is displayed in Figure 9. Both sensing measurement were conducted with the mmID tag boresight relative to the reader system. The chirp parameters of the FMCW radar for all the presented measurements can be viewed in Table I.

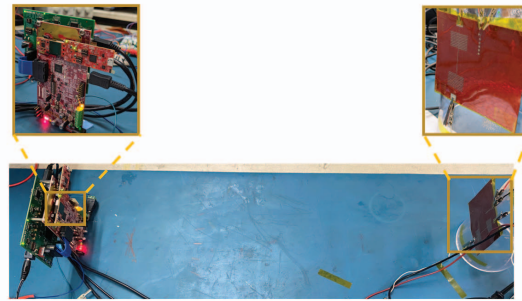


Fig. 9: Measurement setup for simultaneous ranging and flexing of mmID.

The selection of chirp parameters play a crucial role localization of the mmID by establishing maximum reading

range and range resolution of the system. These parameters were optimized to in order to simultaneously localize and sense flexing from the mmID tag. The maximum Intermediate Frequency (IF), and therefore, maximum modulation frequency of the mmID, was 5 MHz due to the sampling rate of 10 MHz, establishing a maximum reading range of 29.997 m. The signal processing framework for simultaneous ranging and sensing is described as follows. First, extraction of the bending sensor information is conducted. This is enabled through a peak search algorithm from the in the image-band from the frequency range of 3.35 MHz to 4 MHz due to the modulation frequency of the mmID f_{mod} being mapped to the level of bending of the sensor. After the negative modulation frequency in the image-band is detected, a positive frequency search window, $W(f)$, defined by

$$W(f) = \begin{cases} 1 & \text{if } abs(f_{Neg}) < f < abs(f_{Neg}) + 250 \text{ kHz} \\ 0 & \text{if } o.w. \end{cases}$$

where f_{Neg} is the detected negative modulation frequency and the 250 kHz is proportional to searching for a single tag at maximum range of 0.75 m from the reader. After identification of both positive and negative modulation frequencies, as described in [3], an estimation of the continuous ranging of the tag from the reader was calculated using the expression,

$$R = \frac{f_{Pos} + f_{Neg}}{2} * \frac{cT_c}{B} \quad (1)$$

, where R , f_{Pos} , f_{Neg} , c , T_c , and B are the range of the mmID, positive modulation frequency of the mmID, negative modulation frequency of the mmID, the speed of light, the total chirp time, and the bandwidth of the chirp respectively. Therefore, through the proposed method simultaneous flex sensing and ranging is enabled for the digital twin sensor node.

A. Flexing Sensor Response at Constant Range

Flex detection experiments were conducted placing the mmID at a constant range 15 cm and adhered to three separate cylinders of radii 2.5, 3.75, and 5.0 separately. During the measurement to view the sensor response, the sensor was continuously flexed to the radius of each cylinder and released. For these measurements, a total of 100 frames were recorded which results in an total measurement time of 4.5 s. An example of the frequency response of the sensor with the largest bending radius can be viewed in Figure 10.

As aforementioned, the peak frequency of this measurement was extracted to enable flex detection of the sensor. The sensor response at different levels of flexing at a constant range is displayed in Figure 11. With a decrease in radius, and therefore, an increase in the amount of bending, there was an expected decrease in the frequency peak extracted based upon the frequency mapping detailed in II-C. Additionally, the sensor response displays stable frequency modulation at the maximum level of bending for each of the measurements and the ability to recover to the starting frequency of the measurement. The ranging of the mmID tag of these measurements

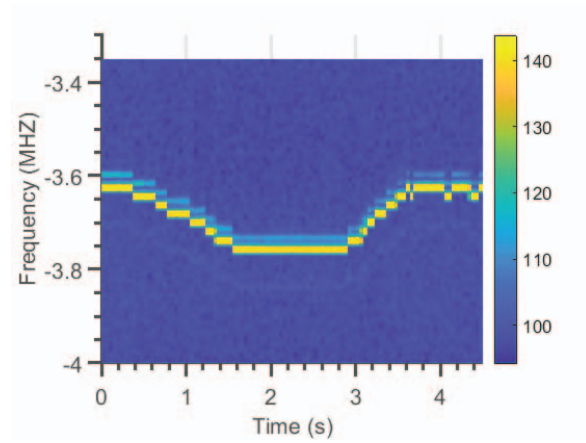


Fig. 10: Frequency of response of sensor over a measurement time.

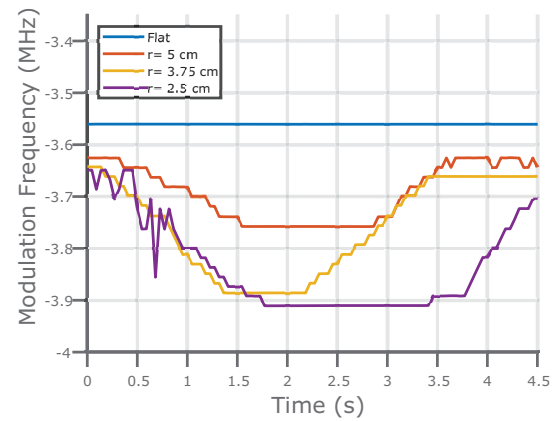


Fig. 11: Frequency Response of each continuous flexing measurement with different bending radii.

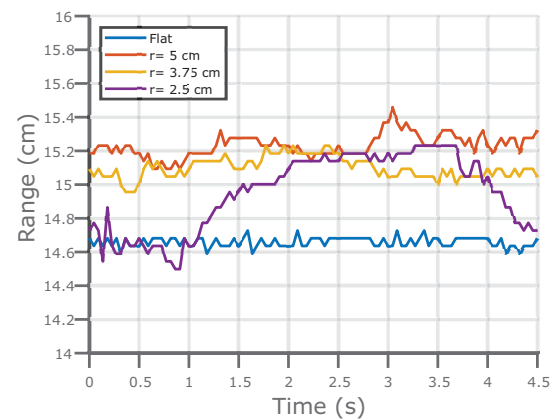


Fig. 12: Continuous estimation of range mmID at 15 cm.

can be viewed in Figure 12. The range measurements display sub-cm level of accuracy with the maximum average error of 3 mm over all the measurements. Thus, the proposed system can accurately detect distinct levels of flexing while accurately measuring the range of the tag.

B. Ranging

Having displayed the the ability to detect different levels of levels flexing while ranging the mmID, the mmID was placed on the cylinder with the largest radius with the same flexing measurement as described in IV-A, but increased ranges from the reader. The results from the sensor response with the same level of flexing at different ranges can be viewed in Figure 13. The sensor response was observed for

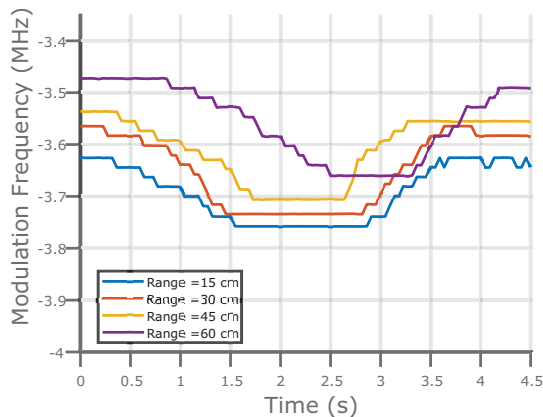


Fig. 13: Frequency of sensor with constant maximum bending radius at different ranges.

all the measurements establishing a maximum reading range of 60 cm from the reader. Additionally, the sensor response displays a decrease in sensitivity with an increase in range. The simultaneous range extraction from these measurements is displayed in Figure 14. These ranging results display again display accuracy within 5 mm accuracy up to 60 cm with a maximum average range error of 3.19 mm. Thus, establishing the ability of the proposed system to simultaneously sense and range a mmID for digital twin applications.

V. CONCLUSION

This paper outlines an effective procedure to manufacture backscatter RF front ends operating in the millimeter wave regime that can be customized for numerous applications in a reliable and low-cost manner using AM techniques. The proposed tag presents a ready-to-use module capable of multi modal sensing using commercially available reader modules. The proposed device is particularly useful in situations where sensing information is required over a given large surface area so that its localization capabilities can be taken advantage of. Additionally, due to the flexible, surface agnostic design and consistent sensor response, new modes of input for wearable Human Computer Interface systems can be envisioned. The

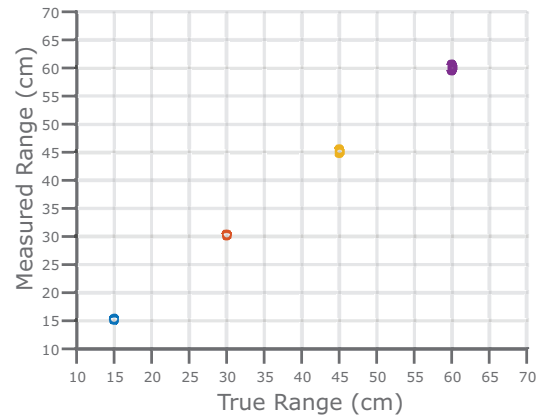


Fig. 14: Estimation of ranging of mmID.

described work could constitute a significant stride forward towards the realization of large-scale deployment of RFID modules for sensing and localization applications in IoT and Digital Twins applications.

REFERENCES

- [1] P. Pursula, T. Vaha-Heikkilä, A. Müller, D. Neculoiu, G. Konstantinidis, A. Oja, and J. Tuovinen, "Millimeter-wave identification—a new short-range radio system for low-power high data-rate applications," *IEEE Transactions on Microwave Theory and Techniques*, vol. 56, no. 10, pp. 2221–2228, 2008.
- [2] P. F. Freidl, M. E. Gadringer, D. Amschl, and W. Bcösch, "mm-wave rfid for iot applications," in *2017 Integrated Nonlinear Microwave and Millimetre-wave Circuits Workshop (INMMiC)*, 2017, pp. 1–3.
- [3] A. O. Adeyeye, J. Hester, and M. M. Tentzeris, "Miniaturized millimeter wave RFID tag for spatial identification and localization in internet of things applications," in *2019 49th European Microwave Conference (EuMC)*, Oct. 2019, pp. 105–108.
- [4] A. Eid, X. He, R. Bahr, T.-H. Lin, Y. Cui, A. Adeyeye, B. Tehrani, and M. M. Tentzeris, "Inkjet-/3d-/4d-printed perpetual electronics and modules: Rf and mm-wave devices for 5g+, iot, smart agriculture, and smart cities applications," *IEEE Microwave Magazine*, vol. 21, no. 12, pp. 87–103, 2020.
- [5] J. Kimionis, S. Shahramian, Y. Baeyens, A. Singh, and M. M. Tentzeris, "Pushing inkjet printing to w-band: An all-printed 90-ghz beamforming array," in *2018 IEEE/MTT-S International Microwave Symposium - IMS*, 2018, pp. 63–66.
- [6] A. O. Adeyeye, R. A. Bahr, and M. M. Tentzeris, "3D printed 2.45 GHz Yagi-Uda loop antenna utilizing microfluidic channels and liquid metal," in *2019 IEEE International Symposium on Antennas and Propagation and USNC-URSI Radio Science Meeting*, Jul. 2019, pp. 1983–1984.
- [7] X. He, B. K. Tehrani, R. Bahr, W. Su, and M. M. Tentzeris, "Additively manufactured mm-wave multichip modules with fully printed "smart" encapsulation structures," *IEEE Transactions on Microwave Theory and Techniques*, vol. 68, no. 7, pp. 2716–2724, 2020.
- [8] R. A. Bahr, A. O. Adeyeye, S. Van Rijs, and M. M. Tentzeris, "3d-printed omnidirectional luneburg lens retroreflectors for low-cost mm-wave positioning," in *2020 IEEE International Conference on RFID (RFID)*, 2020, pp. 1–7.
- [9] J. G. D. Hester and M. M. Tentzeris, "A mm-wave ultra-long-range energy-autonomous printed rfid-enabled van-atta wireless sensor: At the crossroads of 5g and iot," in *2017 IEEE MTT-S International Microwave Symposium (IMS)*, 2017, pp. 1557–1560.
- [10] X. D. Huang, S. M. Bhangale, P. M. Moran, N. L. Yakovlev, and J. Pan, "Surface modification studies of kapton® HN polyimide films," *Polym. Int.*, vol. 52, no. 7, pp. 1064–1069, 2003.